Journal of Innovative Optical Health Sciences
Vol. 13, No. 2 (2020) 2030004 (20 pages)

DOI: 10.1142/S1793545820300049

Photodynamic therapy of brain tumors and novel optical coherence tomography strategies for *in vivo* monitoring of cerebral fluid dynamics

A. Abdurashitov[*,†,§], V. Tuchin[*,†,‡] and O. Semyachkina-Glushkovskaya[*]
[*]*Saratov State University, Saratov 410012*
Russian Federation

[†]*Tomsk State University, Tomsk 634050*
Russian Federation

[‡]*Institute of Precision Mechanics and Control*
Russian Academy of Sciences, Saratov 410028
Russian Federation
[§]*aarkady@me.com*

Received 13 August 2019
Accepted 19 November 2019
Published 21 January 2020

Photodynamic therapy (PDT) is a promising tool for least-invasive alternative methods for the treatment of brain tumors. The newly discovered PDT-induced opening of the blood–brain barrier (BBB) permeability open novel strategies for drug-brain delivery during post-surgical treatment of glioblastoma GBM. Here we discuss mechanisms of PDT-mediated opening of the BBB and age differences in PDT-related increase in BBB permeability, including with formation of brain edema. The meningeal lymphatic system plays a crucial role in the mechanism of brain drainage and clearance from metabolites and toxic molecules. We discuss that noninvasive photonic stimulation of fluid clearance via meningeal lymphatic vessels, and application of optical coherence tomography (OCT) for bed-side monitoring of meningeal lymphatic drainage has the promising perspective to be widely applied in both experimental and clinical studies of PDT and improving guidelines of PDT of brain tumors.

Keywords: Photodynamic therapy; optical coherence tomography (OCT); brain tumor; meningeal lymphatic.

[§]Corresponding author.

1. Photodynamic Therapy (PDT) of Brain Tumors: A Brief History

High grade glioma (HGG) is one of the most common and aggressive brain tumors in adults.[1] However, HGG can be seen in any age group starting from in utero and early infancy through young adulthood.[2–5] In adults, HGG often arises from a low grade glioma that has undergone malignant transformation, but this phenomenon is exceedingly rare in children.[6] Similar to the adults, however, pediatric HGG are characterized by their aggressive clinical behavior and account for a significant amount of morbidity and mortality among children with brain tumors.[7]

HGG typically arise from astrocytic origins, including glial, oligodendrocytes, and ependymal cells.[7] HGGs are classified by the World Health Organization (WHO) as either grade III (astrocytoma) or IV (glioblastoma, GBM), meaning that they are highly malignant tumors with characteristic findings such as hypercellularity, nuclear atypia, and high mitotic activity with or without microvascular proliferation and necrosis.[2,7]

While the median survival time (MST) for patients with GBM has increased since the last study, it is still reported at just 12–18 months following standard therapies including guided surgical resection,[8–11] gamma knife surgery,[12] intensity modulated ionizing radiation therapy,[13] or chemotherapy.[14] In 98%, GBM resection is required to afford long-term benefit to the patients.[10] However, due to the coexistence of normal and malignant brain tissues, complete resection of GBM means sacrificing normal brain tissues. Since the brain functions cannot be substituted by any other sites, GBM resection has to be relinquished to maintain the brain function if the tumor infiltrates the functional areas involved with language, motor functions, senses, vision, and memory. Even, if GBM resection was performed successfully, 80% of GBM recurs within a 2-cm periphery of the initial resection site.[15–17]

Current nonsurgical therapeutic strategies are limited to accessible GBM. The photodynamic therapy (PDT) and photodynamic diagnosis (PDD) are discussed as promising least-invasive tools for the treatment of GBM.

A pioneer in the field of PDT is Niels Finsen, who was awarded the Nobel Prize in 1903 for his discoveries using light in the treatment of cutaneous tuberculosis.[17] PDT first demonstrated by a medical student, Oscar Raab, in 1898 when he discovered the toxic action of acridine on paramecia a unicellular microorganism in conjunction with ambient light.[18] The student worked in the laboratory of Herman Von Tappeiner in Munich who reported in 1904 that the process Raab had described was dependent on oxygen, and Von Tappeiner was the first to use the term PDT to describe the phenomenon of oxygen-dependent photosensitization.[19] Von Tappenier was also the first to perform PDT in humans with skin cancer using eosin as a photosensitizing agent. The physical properties of the hematoporphyrin as a photosensitizer were first described in 1908, and its biological activity was demonstrated a few years later, in 1913, when a German physician, Meyer-Betz, injected himself 200 mg of hematoporphyrin and remained sensitive to light for 2 months.[20] In modern history, Dougherty,[21] Wilson,[22] Stepp,[14] Krasnovsky,[23] Uzdensky,[24] Zavadskaya,[25] Shafirstein,[26] Hasan[27] are well-known researchers in experimental and clinical studies of PDT.

PDT is a form of therapy that combines a light source and nontoxic photosensitizing agents (photodynamic dyes). The systematically or topically administered photosensitizer is specifically accumulated in tumor tissue. When the concentration of photosensitizer is sufficient, it is activated by exposure to light appropriated for its excitation. The excited photosensitizer interacts with molecular triplet oxygen ($^3O_2$) and produces singlet oxygen ($^1O_2$) resulting in tissue oxidation. The mechanisms of $^1O_2$ generation are the light-induced transition one of electrons in a higher-energy orbital from the ground state (triplet oxygen) in a short-lived ($\tau_{fl} = 10^{-6}$–10^{-9} s) electronically excited state (singlet oxygen) (Fig. 1(a)). The $^1O_2$ damages tumor cells by direct injury (necrosis and apoptosis) or due to the occlusion of tumor vessels (thrombus formation), and secondarily enhanced host immunity.[28,29] The life of $^1O_2$ is between 0.04 and 4 μs and the distance of migration between 0.02 and 1 μm. Therefore, PDT is considered a min-invasive therapy targeting each cell containing the photosensitizer alone while preserving the adjacent normal tissues (Fig. 1(b)).

PDT has been investigated as an adjuvant for the treatment of GBM for approximately 35 years.[30–35] In 1980, Perria *et al.*[36] performed the first-in-man study of PDT using Photofrin®

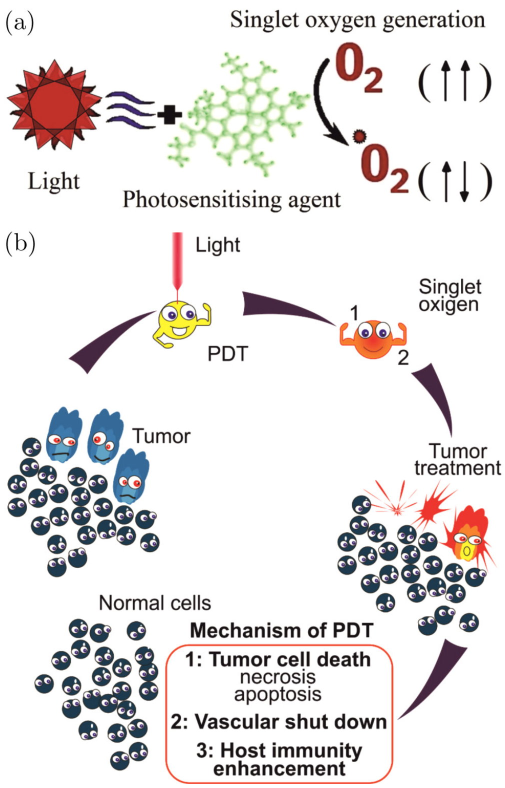

Fig. 1. Mechanisms of singlet oxygen generation (a) and PDT-mediated damage of tumor cells (b).

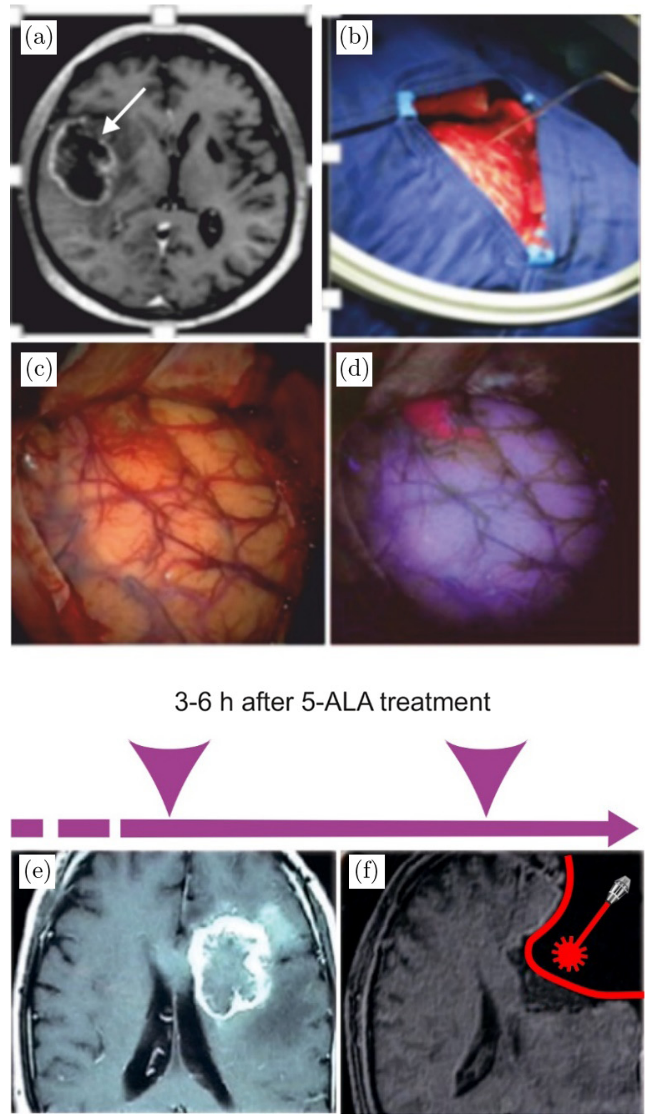

Fig. 2. The fluorescence guided resection of GBM in patient: (a) magnetic resonance imaging (MRI) of glioblastoma (arrowed); (b) preparation of surgical area; (c) the surface of brain after craniectomy; (d) specific fluorescence of 5-ALA in ultraviolet 3–6 h after 5-ALA administration per os; (e and f) PDT of GBM, where e — MRI of GBM and f — schematic illustration of post-surgical PDT of GBM. Panels (a)–(d) presented with the permission of Herbert Stepp, University Hospital of Munich, Germany. Panels (e) and (f) were adapted from J. Akimoto, "Photodynamic Therapy for Malignant Brain Tumors," Neurol Med Chir (Tokyo) 56, 151–157, 2016.

(5 mg/kg, light density 720–2400 J/cm^2) on eight patients anaplastic astrocytoma and GBM. Later, in 2005 Kaneko[37] and Stylli *et al.*[38] conducted PDT with Photofrin® (5 mg/kg, light density 70–240 J/cm^2) and a combination of radiochemotherapy in 145 patients with GBM. They reported MST 14.9 months for patients with initial GBM and 13.5 for patients with recurrence. In 2006, Muller *et al.*[39] treated 112 patients with GBM by PDT (Photofrin® (2 mg/kg, light density 20 J/cm^2) and demonstrated MST 11 months for PDT-group and 8 months for the control group. In the same year, Kostron *et al.*[40] conducted PDT using Foscan® (0.15 mg/kg, absorption wavelength 652 nm, 20 J/cm^2) for patients with recurrent GBT and reported that MST was 9 months for the PDT-group vs. untreated patients. In 2007, Stepp *et al.*[14] used the pro-drug 5-aminolevulinic acid (5-ALA, 20 mg/kg) for PDD of GBM. For PDD a specific fluorescence of 5-ALA was studied in ultraviolet 3–6 h after administration per os (Figs. 2(a)–2(d)). This group also used PDT for patients with GBM (laser 635 nm with 100, 150, and 200 J/cm^2) and showed MST 6 months for the PDT-group compared with the control group.

The most successful results have been shown by Eljamel *et al.*[41] in 2010, who performed PDT in 27 patients with GBM using (Photofrin®, 2 mg/kg, light density 100 J/cm^2) and reported that MST was 53 weeks in the PDT-group and 24 weeks for the control group, i.e., survival rate was increased by 1.5 year. For a more detailed discussion of clinical results of PDT for HGG, Bechet *et al.*[33] and Quirk *et al.*[34] give an excellent overview.

2. PDT-Induced Opening of the Blood–Brain Barrier and Vasogenic Edema

The traditional explanation of the anti-cancer PDT effect is $^1O_2$-induced damage of the endothelial cells resulting in tumor microvasculature collapse.[42,43] However, in recent several studies have been shown completely new vascular mechanisms of PDF such as an increase in the blood–brain barrier (BBB) permeability[44–50] (Fig. 3).

The physical BBB form three elements: endothelial cells, embedded with them pericytes, and covering them astrocyte end-feet. The diffusion BBB presented by a complex of intra- and trans-membrane proteins.[51,52] Tight junctions (TJs) are located on the apical membrane of cerebral endothelium and contain the family of claudins, occludin, junctional adhesion molecules as well as in the cytoplasm of endothelial cells including zonula occludens proteins (ZO-1, ZO-2, ZO-3, and cingulin) bound to actin cytoskeleton.[53–55] Adhesion junctions are located at the part of the basement membrane of the paracellular space and are composed of cadherin, integrin and their associated proteins.[56]

The BBB plays an important role in the central nervous system (CNS) health controlling penetration of blood-borne agents into the brain and protects the CNS from toxins and pathogens.[57] However, it also limits the delivery of therapeutics to CNS that poses a challenge for effective therapy to majority of CNS diseases.[58] Therefore, the methods for the BBB opening have received significant attention in the last decades.[59–62]

Recently, it has been revealed that PDT, as a widely used tool for therapy of GBM,[14,30–41] can also effectively and site-specifically open BBB.[44–50] Hirschberg[44] using 400 μm bare flat-end quartz fiber (635 nm) and stereotaxic procedure clearly show that the ALA-PDT causes the opening of BBB. At the low fluence levels of 9L, the ALA-PDT opens the BBB rapidly without any damages of brain tissues, the disrupted BBB is observed during 2 h following PDT and restored during the next 72 h.[44] The disruption of BBB is greater using the higher fluence level of 26 J but the damages of surrounding tissues (necrosis, edema, hemorrhage) are observed 17 days.

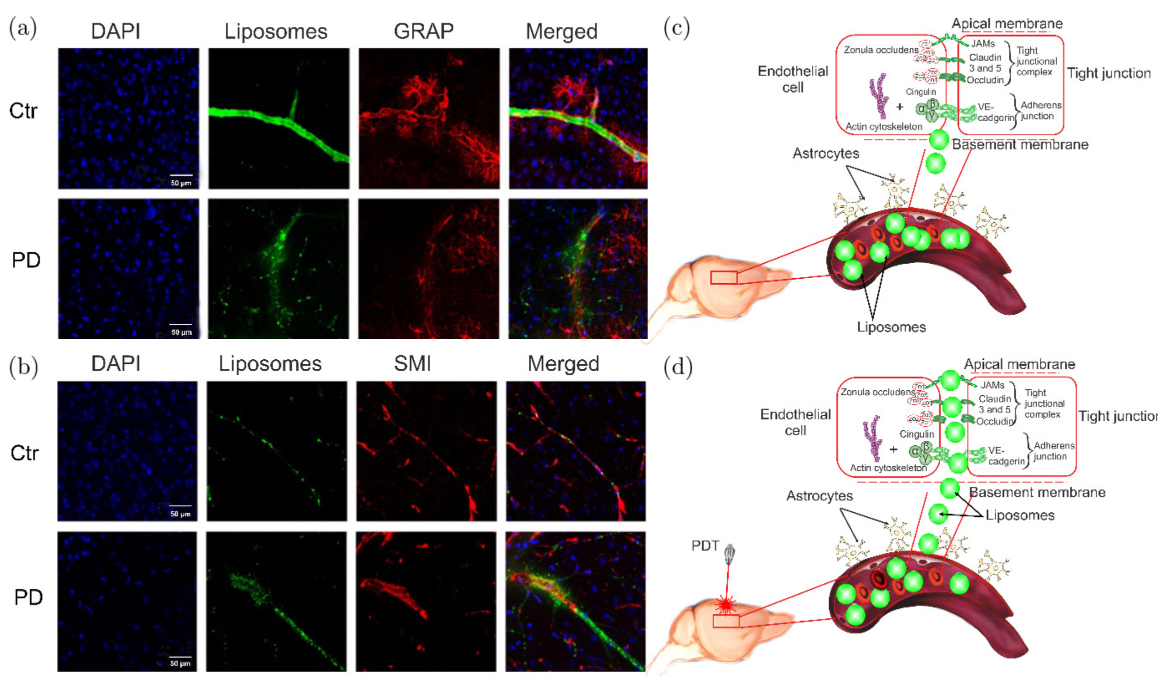

Fig. 3. The confocal imaging of noninvasive PDT-induced BBB opening for liposomes with usage of markers of neurovascular unit: (a) liposomes distributions between the astrocytes labeled by antibodies of astrocytes (GFAP); (b) liposomes leakage outside the vascular endothelial cells labeled by antibodies of cerebral endothelium (SMI); PD — photodynamic effects, Ctr — the control group. The white arrows show the sites of liposomes leakage; (c and d) — schematic illustration of PDT-opening of the BBB.[43]

We confirmed these results in our work.[48–50] Using laser 635 nm (10–40 J/cm^2, 40–100 mV, 250–400 s) and 5-ALA (NIOPIK, Russia, 20 mg/kg, i.v.) we showed opening of the BBB to fluorescent liposomes and for high weight molecular molecules in the middle dose of laser influences on the brain tissues (15–20 J/cm^2, 40–60 mV, 375–333 s) (Fig. 3).

Several authors show the efficiency of PDT-related BBB disruption for targeted macrophages migration from blood into the brain with the aim to improve PDT of glioma using macrophages as transport system through the BBB for gold-nanoparticles.[39–41] The nanoparticles show great promise for PDT.[63] Madsen in an experiment in vivo showed that PDT (the photosensitizer — aluminum phthalocyanine disulfonate (AlPcS2a), $\lambda = 670$ nm; light dose = 2.5 J) is effective for the opening of BBB and the migration of systemically administered exogenous macrophages loaded with iron oxide nanoparticles (120–180 nm) in the brain of rats.[45] Trinidad in experiments in vitro using macrophages loaded gold nanoparticles (120 nm) and human FaDu cancer cell line (head and neck squamous cell carcinoma) showed reducing 2-fold the cell viability after PDT (AlPcS2a-mediated $\lambda = 670$ nm, fluence level 0.25 J/cm^2) combined with photothermal therapy ($\lambda = 810$ nm, at 14 W/cm^2 irradiance).[64]

The mechanisms responsible for PDT-mediated increase in BBB disruption remain poorly understood. Some reports show that PDT has effects on the endothelial cells resulting in the increasing gaps between endothelial cells via changes of the cytoskeleton, cell rounding and constriction loss due to microtubule depolarization.[65–67] The singlet oxygen ($^1O_2$) generated during PDT causes endothelial regulation imbalance of vascular relaxation. Thus, the vascular resistance to photo-induced oxidative stress decreases, resulting in the redistribution of calcium, reduction of influx and calcium release from intracellular storage.[68–71] In our study,[48,49] using markers of neurovascular units such as SMI (the vascular endothelial cells), laminin (the basal membrane), and GFAP (the astrocytes), we show their disorders resulting in an increase of the BBB permeability, therefore, the tested tracer (dextran, 70 kDa or liposomes) passed through the vascular endothelium and the basal membrane with further distribution between astrocytes (Fig. 3).

Our results uncovered the elevated expression of ARRB1 that is the marshal in signaling transmembrane processes, and decreases in the expression of CLND-5 and VE-cadherin as main components of BBB integrity.[52,72,73] We assume that the ARRB1 induced the internalization of CLND-5 and VE-cadherin, accompanied by the loss of surface on these proteins in space between endothelial cells, which can be one of the mechanisms underlying PD-induced opening of BBB for liposomes. Our hypothesis is based on the results of other experiment demonstrating the mechanism of BBB disruption via ARRB2-mediated internalization of VE-cadherin induced by vascular endothelial growth factor (VEGF). The elevated expression of ZO-1 during PD-mediated opening of BBB on the background of lowered expression of CLDN-5 and VE-cadherin could also suggest disordered interactions of TJ proteins.[74] Our results are consistent with data of other research showing that PDT has a direct effect on increasing the gaps of the TJs between endothelial cells via changes of the cytoskeleton, vascular tone loss due to microtubule depolarization.[75]

In our work, we used 5-ALA, which is a porphyrin precursor. One of the mechanisms by which porphyrin causes PDT effects is an elevation of expression of heme-transport protein (HCP1), which is capable of transporting porphyrin compounds. Recently, it has been shown that HCP1 expression is associated with increased reactive oxygen species production and hypoxia[76] that we observed in our work. We suppose that PDT-induced increase in oxidative stress associated with mild hypoxia and changes in TJ and adherens junction proteins might be one of the mechanisms underlying PD-related BBB opening for liposomes.

While PDT results in direct phototoxic tumoricidal effect, it also has been shown that PDT can cause a variety of vascular effects ranging from transient vasospasm, increased vessel leakiness, and vessel wall disintegration ending in vessel closedown.[77–80] In this context, PDT induced vessel leakage has been reported to induce significant brain edema by a variety of photosensitizers.[81–83]

Our data also demonstrate that there are age differences in PDT-related opening of the BBB (Fig. 4). The cerebral vessels of 4 weeks old mice are more sensitive to PDT-mediated changes in the

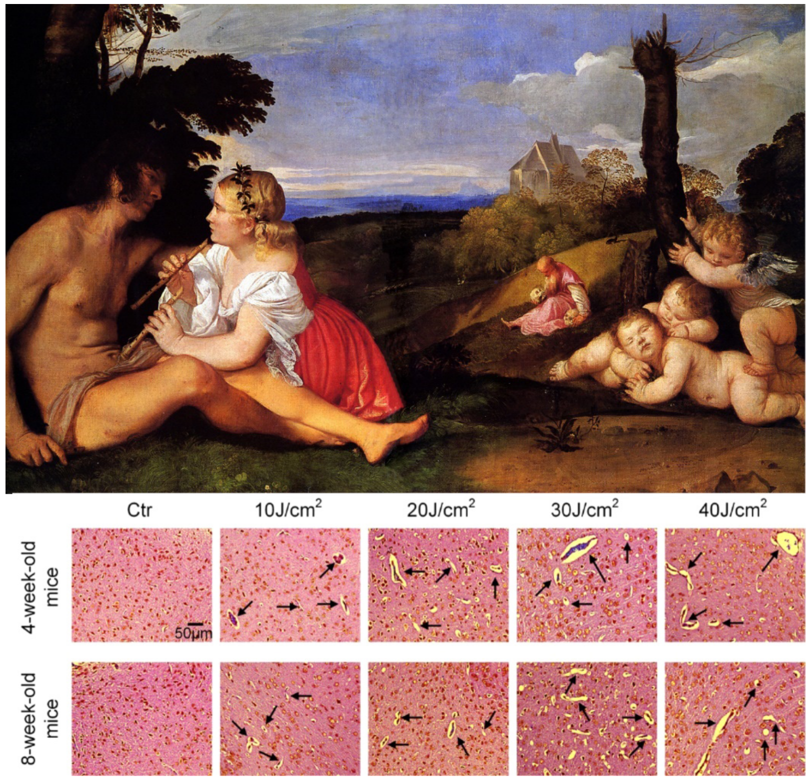

Fig. 4. The illustration of age differences in PDT-induced opening of the BBB. Histological analysis clearly demonstrates that PDT-induced opening of the BBB is accompanied by brain edema in laser fluence depended manner that is more pronounced in juvenile mice compared with adult mice. Ctr – the control group, no solute leakage; laser (10–20–30–40 J/cm^2) causes the perivascular edema (black arrows), which looks as empty spaces around cerebral vessels.[48]

BBB permeability compared with 8 weeks old animals. The young mice demonstrated more significant increase in the leakage of Evans Blue and 70 kDa FITC-dextran after application of low and middle doses of laser (10–30 J/cm^2) that accompanied by the development of more pronounced perivascular edema. The formation of vasogenic edema after PDT also has been shown in other works.[44,83,84] One of the mechanisms responsible for extensive fluid accumulation in the perivascular space (PVS) of brain is disruption of TJ complex and imbalance in the control of expression of aquaporins channels in the astrocytes and the vascular endothelium.[85,86]

The newly discovered effects of PDT on the BBB permeability open novel strategies for drug-brain delivery, especially for post-surgical treatment of GBM. The novel understanding of age-differences in PDT-mediated opening of the BBB and associated with this vasogenic edema is an important data for better understanding of mechanisms underlying cerebrovascular effects of PDT-related fluorescence guided resection of brain tumor and for improving guidelines for PDT of GMB.

3. PDT-Mediated Opening of the BBB and the Meningeal Lymphatic System

The main function of the lymphatic system is the fluid drainage, i.e., to return the excess of the interstitial or extracellular fluid back to the venous circulation. However, the situation with the brain is different due to the presence of the BBB that limits the entrance of fluids, molecules, and cells into the brain parenchyma. Over two centuries there was a dogma about the isolation of the brain from the immune system due to the lack of the lymphatic vessels within the CNS.[87–97] Nevertheless, the literature is filled with findings of a physiological relationship between the brain drainage and the lymphatic system of head and neck.[87–103] The rediscovery of the meningeal lymphatics and finding of the presence of the lymphatic vessels in the brain tissues gave a new impulse in the reassessment of classical explanation of the role of the lymphatics in the brain drainage.[98,104,105] In these studies, which were performed on rodents and human brain, it was clearly demonstrated that the meningeal lymphatic vessels are localized along the main cerebral venous sinus and express all of the molecular hallmarks of lymphatic endothelium.

In our study, we tested the hypothesis about the recruitment of the meningeal lymphatics by the BBB opening and that these changes are an important for stimulation of the brain drainage and clearing (Fig. 5). We used two methods for the BBB opening — the sound that induces the mild BBB opening and PDT causing the strong BBB leakage with the accumulation of extensive fluids in the PVS.[106,107] Indeed, using confocal imaging of dextran extravasation and spectrofluorimetric assay of Evans Blue albumin complex level in the brain tissues, we showed opening of the BBB for these tracers that was more pronounced in the PDT group vs. the sound group. These changes stimulated the

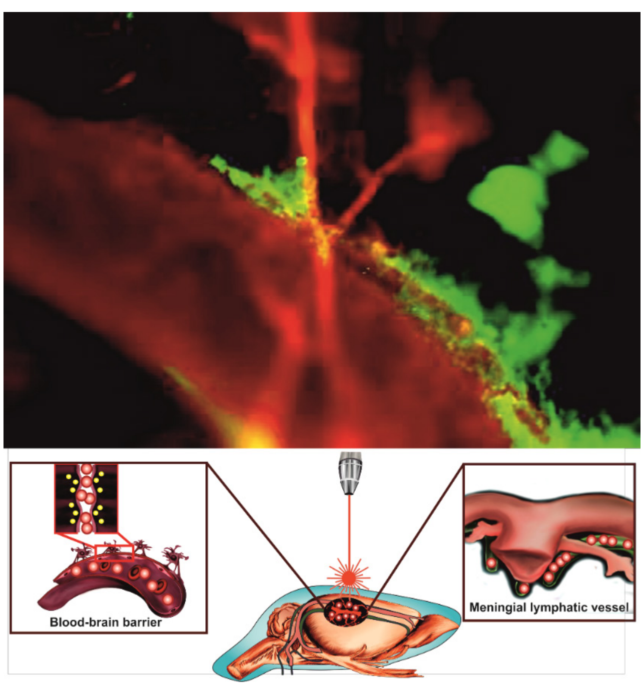

Fig. 5. (Color online) Fluorescent microscopy of clearance of FITC-dextran (red color) from the brain via the meningeal lymphatic vessels (green color, labelled by specific antibodies LYVE-1 conjugated with Alexa 488). The FITC-dextran injected intravenously immediately is observed in the Sagittal sinus (the main cerebral vein) and after PDT-opening of the BBB it is also presented in the meningeal lymphatic vessels due to activation of clearance of FITC-dextran from the brain parenchyma.[107]

brain drainage with an increase in the volume of cerebral spinal fluid (CSF) in the cisterna magna that was also more pronounced in the PDT group vs. the sound group. The BBB-mediated activation of the brain drainage can be explained by the hypothesis of Monro and Kellie.[108] The constitutions of the brain (the blood, CSF, intestinal fluid) create a state of volume equilibrium such that any increase in the volume of one of the cranial constitutions would be compensated by a distribution of the volume of another. The BBB opening is accompanied by an influx of fluids and different molecules in the brain tissues that in some cases (PDT-induced opening of the BBB) causes the vasogenic edema or accumulation of extensive fluids in the brain parenchyma. We assume these changes stimulate the brain drainage of fluids in a way to keep the extracellular homeostasis. Our results clearly show that PDT caused the strong the BBB leakage that was associated with vasogenic edema and with a significant increase in the CSF volume in the cisterna magna vs. the control group. The mild BBB disruption by sound was not associated with visible (histological data)[106] changes in the PVS and the changes in the CBF volume in the cisterna magna were within a normal range.[109] We hypothesize that mild changes in the BBB might be completely compensated by an activation of the brain drainage and clearing system as in the case with sound-related opening of the BBB. While a strong BBB leakage (PD-induced opening of the BBB) causes a quick and significant fluid influx in the brain parenchyma that cannot be compensated immediately by the drainage system of the brain and requests a longer time for recovery.[110]

Our results confirmed the hypothesis about the recruitment of the meningeal lymphatics and its involvement in the brain drainage. So, the comparison between the PDT/sound groups clearly demonstrates that opening of the BBB is accompanied by significant an increase in the diameter of the meningeal lymphatic vessels that is equivalent to the intensity of BBB disruption and to the CSF accumulation in the cisterna magna. The changes in the lymphatic vessels associated with the BBB opening might be explained by the similar structure of the lymphatic vessels and the BBB. Indeed, the lymphatic vessels are composed by TJ proteins such as claudin-5, a family of ZO proteins, endothelial selective adhesion molecule; adherents junction proteins (VE-cadherin); junctional adhesion molecule-A and PECAM-1/CD31.[111,112] The opening of the BBB is accompanied by disbalance in expression of indicated proteins[113] that can influent the complex of these proteins in the lymphatic system. However, this hypothesis requires further more detailed studies for confirmation. The activation of nitric oxide (NO) production in the lymphatic endothelium might be a reason of increasing of the diameter of the meningeal lymphatic vessels after opening of the BBB. The NO is responsible for the reduction in the tone of the lymphatic vessels via opening of ATP-sensitive $K(^+)$ channels.[112,114–117] The impact of NO on lymphatic tone has been extensively studied using pharmacological modulation of NO synthase.[112,114,118,119] However, the NO effects on the lymphatic endothelium strongly depend on the initial conditions.[117,120] The relaxation of the lymphatic vessels also depends on the oxygen level in the lymphatic system. The low oxygen tension (8–35 mmHg) in lymphatics vs. surrounding tissues promotes an increase in NO bioavailability and dilation of the lymphatic vessels.[115]

We also revealed that the meningeal lymphatics is the pathway in the brain clearing. Indeed, confocal imaging showed the presence of dextran in the meningeal lymphatics after its crossing of the BBB from the blood and accumulation in the brain parenchyma. Aspelund *et al.* also showed the involvement of the meningeal lymphatics in the brain clearing from high weight molecules.[104] This group was not focused on the study of interaction between the BBB and the meningeal lymphatics but they used injection of tracers directly into the brain parenchyma that might destroy the BBB structure and stimulate brain drainage as well.

Although that the important role of the nasal and cervical lymphatics in the brain drainage has been discussed by Schwalbe,[100] Cserr and Knopf,[97] Kida *et al.*,[91] Koh *et al.*,[96] Abbott,[94] and more recently by Aspelund *et al.*[104] and Louveau *et al.*,[105] no the anatomical pathway for brain drainage has been clearly demonstrated. It is more likely that the meningeal lymphatics and probably obtained recently the cerebral lymphatic vessels[98] are most prominent pathway for the lymphatic drainage of brain fluids and the connective bridge between the meningeal/cerebral and peripheral lymphatics (Fig. 6).

These data shed light on the role of the meningeal lymphatics in the mechanisms underlying the neuropathology and open novel strategies for a noninvasive stimulation of lymphatic brain drainage, which is also discussed by Kipnis's group.[121]

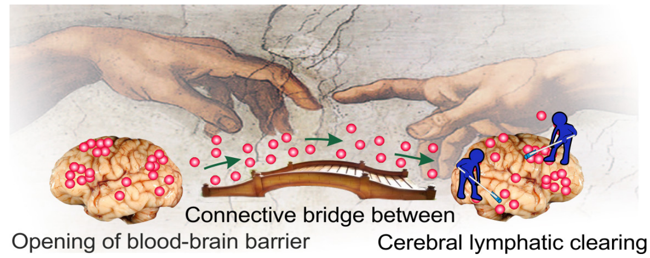

Fig. 6. The schematic illustration of function of meningeal lymphatic system. The molecules crossing the opened BBB eliminate from the BBB via the meningeal lymphatic system.

The better understanding of the physiology of the lymphatics in the brain will give new knowledge about the role of lymphatics in the rehabilitation of the brain functions after neural pathologies. The ability to stimulate lymph flow in the brain is likely to play an important role in developing future innovative strategies in neurorehabilitation therapy.

However, there is no clinical technique and only a few expensive approaches in experiments for the study of functions of the meningeal lymphatic system that limits a progress in this field. Two-photon microscopy is used for the study of behavior of fluorescent meningeal lymphatic vessels in transgenic mice, which are expensive and not widely available for the experimental work.[104] MRI of meningeal lymphatics is also proposed as a novel method for in vivo study of meningeal lymphatics.[122] But, this method does not give good images due to the very small size of meningeal lymphatic vessels even in human and monkey. MRI is not a bedside technique and cannot be used widely in clinics and experiments. Therefore, development of novel tools for in vivo study of functions of meningeal lymphatics is an actual and urgent problem in neurophysiology.

4. Optical Coherence Tomography for *in vivo* Imaging of Meningeal Lymphatic System

Optical coherence tomography (OCT) is a widespread tool for *in vivo* imaging of tissues.[123,124] By being an interference technique it detects the interference pattern (coherent sum) of reference light and light that was backscattered from the sample. Due to low coherence property of a used light source only light that being directly reflected from a narrowly localized volume (known as coherence volume) from the sample arm involved into the interference formation. This process is the same as in a traditional confocal microscope, where two physical conjugated apertures are used to block unwanted light from entering the detector. The more optical frequencies are used to form an interference signal, the better is the axial resolution. Mathematically this wrote as:

$$l_c \approx \frac{\lambda_0^2}{\Delta\lambda}, \tag{1}$$

where l_c is the length of coherence volume is axial direction, λ_0^2 and $\Delta\lambda$ are the central wavelength and spectral bandwidth of the light source respectively. For a transverse resolution the formula is the same as for a classical bright-field microscope

$$\mathrm{res}_{x,y} \approx 0.61\frac{\lambda_0}{\mathrm{NA}}, \tag{2}$$

where λ_0 is the central wavelength of a light source and NA is the numerical aperture of a used lens. It is a unique property of an OCT system to unbound axial and transverse resolution from one another thus axial resolution is independent of a used lens.

In present time OCT system usually divided in two types: less common time-domain and widely used spectral-domain (SD).

In a rough approximation, from an OCT point of view the sample is just a combination of elementary reflective layers (refractive index inhomogeneities) distributed along the depth axis of the sample. A light wave that being reflected from a particular depth is then coherently combines with the reference wave. Such process is repeated for all elementary reflective layers.

In time-domain systems such detection is achieved by mechanical movement of a reference mirror to match the optical path delay between sample and reference mirror. This is rather slow and tedious procedure (from the point of view of phase stability and repeatability of the motion) so comes the new detection scheme which implies operation in spectral domain to perform detection of spectral properties of the OCT signal.

It should be pointed out that with depth the phase delay between sample wave and reference wave is increasing. This means that deeper layers produce interference fringes with progressively higher frequencies. It is convenient to think of an OCT signal as a superposition of such oscillations with different frequencies, mathematically this can be written as

$$I(k) = S(k)|e^{-inkz_i} + e^{ikz_{\mathrm{ref}}}|^2, \tag{3}$$

where $I(k)$ is the intensity distribution at the spectrometer detector, $S(k)$ is the spectral intensity distribution of a light source, k is a wave number, n is the refractive index of a sample, z_i and z_{ref} are elementary reflective layer position and reference mirror position relative to the given origin. Equation (3) looks like a Fourier transform of a spectral intensity distribution, isn't it? From this observation such types of OCT is also known as Fourier domain ones. To reconstruct the depth resolved signal, also known as A-scan, inverse Fourier transform of Eq. (3) should be taken.

Both structural and functional information about the specimen can be extracted from the OCT signal.[123–128] There are two major types of OCT systems commercially available on the market: SD and swept-source (SS). SDOCT is based on a broadband light source, typically super luminescent diode (SLD) and spectroscopic device to perform parallel (relative to wave-number) detection of the interference signal in a frequency domain.[129] High acquisition rates can be achieved with this setup but the detection scheme of SDOCT implies some fundamental limitations on the signal. The finite resolution of the spectroscopic device impaired with a linear array of evenly spaced photodetectors contributes the most to the well-known SDOCT signal "fall-off."[130] This assumption is made for low-NA scanning lenses, which is usually the case of a conventional OCT system. In a case of high-NA objectives (referred as OCM[131]) focusing on a particular range of depths is required for optimal performance due to low depth-of-field of such lenses. Opposed to the SDOCT, SS systems use a swept source laser with a relatively narrow spectral line which can be swept across a finite range of frequencies. The intensity of an interference pattern at particular narrow optical frequency band is then detected by a single photodiode, thus greatly reduces the "fall-off" effect with a trade-off of less acquisition speed compared to the SDOCT systems.

Lymph fluid due to its relatively high transparency in a broad spectral range and low concentration of lymphocytes is barely can be imaged by an OCT system. Besides that, the meningeal lymphatic system consists of fairly small vessels of order of the tenth microns,[100] thus required a high NA objective and dense lateral scanning to properly sample them. Perspective way to overcome such concerns is to introduce some sort of contrast agent into the lymph fluid to increase number of ballistic photons reflected from lymphatic vessel flow. Composite gold nanorods (GNRs) are widely used particles for such purpose.[132] By adjusting their length and diameter, the plasmon resonance can be precisely tuned to match the central wavelength of the OCT's light source.

Advanced methods of OCT signal processing based on the intensity and phase analysis as well as sophisticated protocols for spectroscopic OCT[133–135] were developed recently to compute the distribution of GNRs within tissues and enhance OCT signal from the small blood vessels.

For intensity and phase angiography approaches GNRs serves the same role as red blood cell (RBCs) in a regular blood vessel — time-varying inhomogeneity with random intensities and phases of the scattered light. As a result of such interactions, dynamic speckles arise within the vessel to which an extensive set of micro-angiography algorithms can be applied.[136]

The detected quantity in the SD or SS OCT is the spectrum of the interference pattern. Due to strong plasmon absorption and scattering, GNRs will induce spectral changes in the light backscattered from the sample. By performing spectroscopic based signal processing it is possible to enhance the detection sensitivity of GNRs.[135] Another approach is to apply a spectral mask to limit the spectral band for OCT signal reconstruction to one that fits closely to the peak of plasmonic extinction for better sensitivity, but in a trade-off of axial resolution.

The example of meningeal lymphatic vessels (indicated by arrow) is shown in Fig. 7 without (left frame) and with (right frame) presence of GNRs inside the lymphatic fluid. In the white rectangle, there is a blood vessel with strong OCT signal and notable shadowing "tail" beneath due to the multiple scattering in a large fraction volume of RBCs.

These images were obtained using GANYMEDE, Thorlabs Inc. OCT system with technical characteristics listed in Table 1.

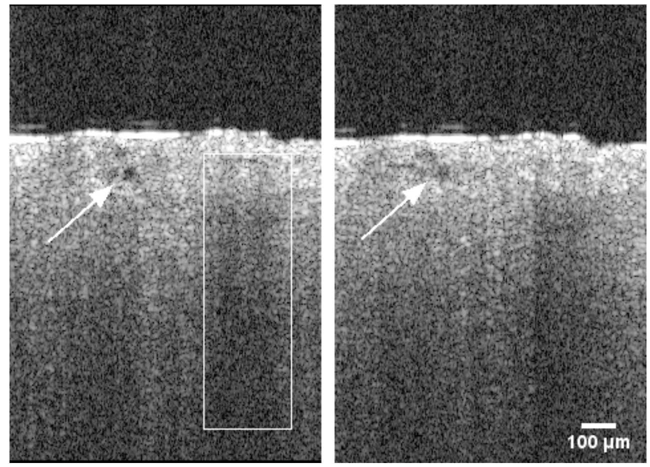

Fig. 7. Effect of GNRs presence inside a lymphatic fluid on OCT signal. There is a strong signal rise after the injection of GNRs (right panel) due to increased scattering from within the lymphatic vessel. The lymphatic vessel is marked by an arrow; blood vessel is marked by the white rectangle.

Table 1. Technical specifications of the GANYMEDE OCT.

GANYMEDE OCT, Thorlabs inc.	
Central wavelength	930 nm
A-scan rate	30 kHz
Imaging depth (theoretical maximum)	2.7 mm
Axial resolution (water)	4.4 μm
Transverse resolution (theoretical maximum)	12 μm
Field of view (FOV)	3.2 mm × 3.2 mm

5. OCT Analysis of Cerebral Blood Flow and Lymphatic Drainage in Malignant Brain Tumor During Photomodulation

If for some reasons brain lymphatic vessels could not be imaged directly, it is still possible to detect the modulated response indirectly by monitoring fluid in the lymphatic nodes outside the brain.

A B-mode OCT scan of a well-developed deep lymphatic node is shown in Fig. 8. Many voids with background level of OCT signal can be located on this image. By injecting GNRs in the cortex they will be collected by the lymphatic drainage system and guided outside the brain directly into the lymphatic nodes at a specific rate which can be modulated by either laser or other stimuli. As the concentration of GNRs inside these voids increases so does the OCT signal. In Fig. 9 OCT signal from

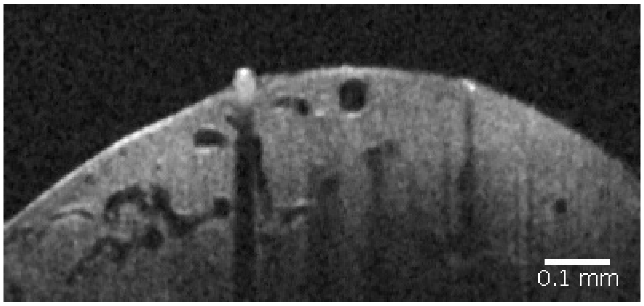

Fig. 8. OCT image of deep lymphatic node.

the void became comparable with OCT signal of surrounding static tissue in 60 min after intra-cortex injection when concentration of nanoparticles significantly increased.

Micro-angiography techniques became the most popular methods for blood vessels mapping in OCT.[126,136] Unlike Doppler protocols[125] they are angle free, robust and easy to implement. In general, they are based on the analysis of the time-variant intensity of speckle structures, produced by a moving RBCs within the vessel. Standard scanning protocol employs a number (usually 4) of consecutive B-scans in the same spatial location of the sample at some time interval. A variance of intensity fluctuations at each pixel of these B-scans is computed using the following equation:

$$\sigma = \sqrt{\frac{1}{N-1}\sum_{N}(I(x_N, z) - \bar{I})^2}, \qquad (4)$$

where N is the number of B-scans in the same location, $I(x_N, z)$ is the instantaneous intensity of a given pixel, $\bar{I}$ is the mean intensity of a given pixel. Since it is an intensity based approach, it is very important to correctly adjust the histogram of raw B-scans to achieve maximum sensitivity. Here a semi-automatic algorithm for histogram adjustment based on noise analysis inside a region of interest (ROI) was shown. Histograms of the whole B-scan and the noise ROI were plotted in Fig. 10.

Maximal value of background noise histogram was then used as a threshold to adjust the histogram of a whole B-scan, namely its intensity values was mapped in a range of $[P_{\max}(\text{noise}), 1]$, where $P_{\max}$ is the most frequent intensity of the noise (vertical red line in Fig. 10). Figure 11 shows the raw B-scan (left panel) and an adjusted B-scan (right panel).

This procedure is done to eliminate small noise signals which fluctuate with time and may cause unambiguous results after computing speckle variance. To see the effect of such histogram correction speckle variance maps were computed using Eq. (1) before and after applying the intensity correction algorithm. Results are presented in Fig. 12.

Because of high noise inclusion in intensity fluctuations, their variance is masking the variance of speckle pattern and no useful data can be extracted. In contrast to that, after the application of intensity adjusting algorithm most of the noise is mapped to 0 and, therefore, no masking is occurred. Bright

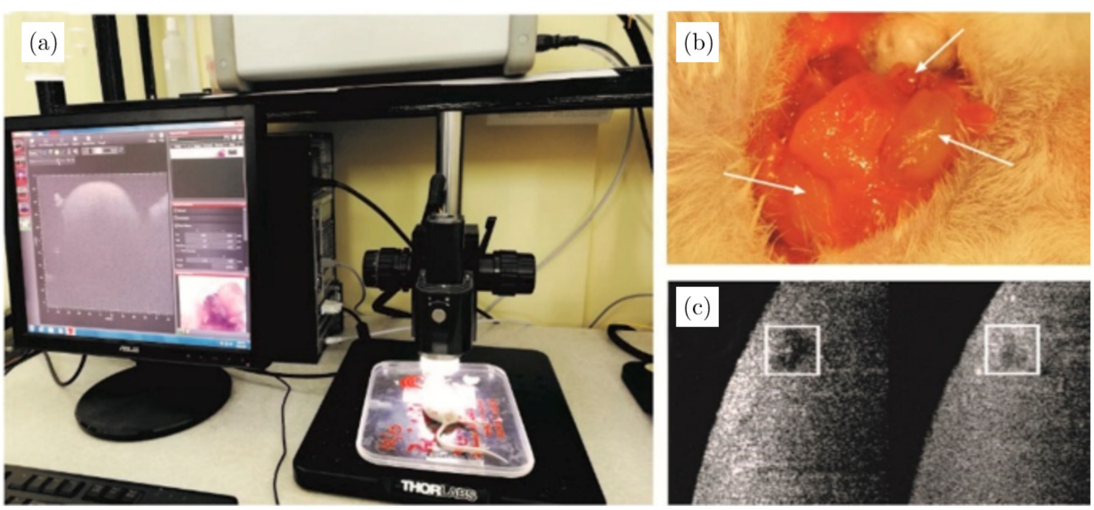

Fig. 9. Time-dependent B-scan intensity changes as the local concentration of GNRs increases: (a) scheme of OCT measurement of GNRs accumulation in deep cervical lymph node; (b) anatomical position of the deep and superficial cervical lymph nodes in the neck of mice; (c) example of OCT image of deep cervical lymph node before and 60 min after the start of OCT recording (more bright square means a bigger concentration of GNRs in the deep cervical lymph node).

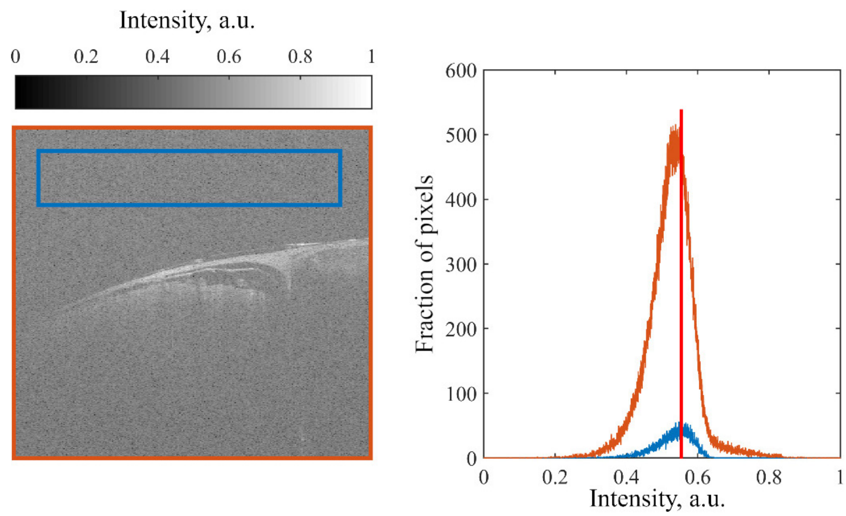

Fig. 10. A comparison between whole B-scan histogram and a histogram of background noise.

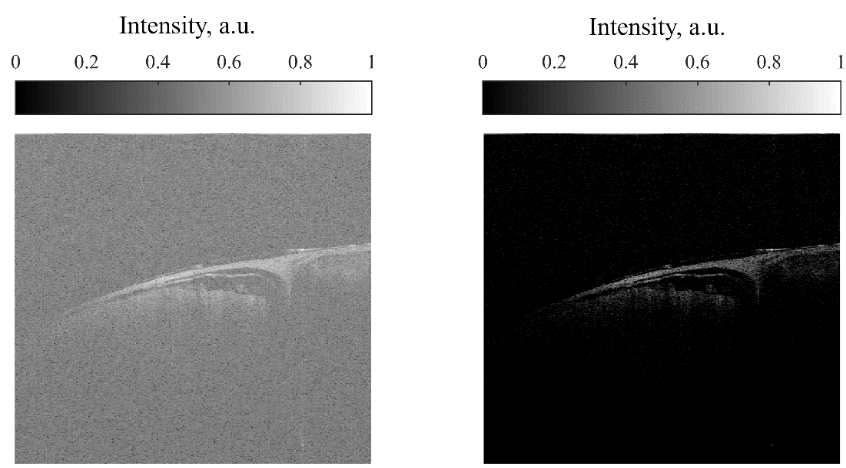

Fig. 11. Raw — left and intensity adjusted — right B-scan.

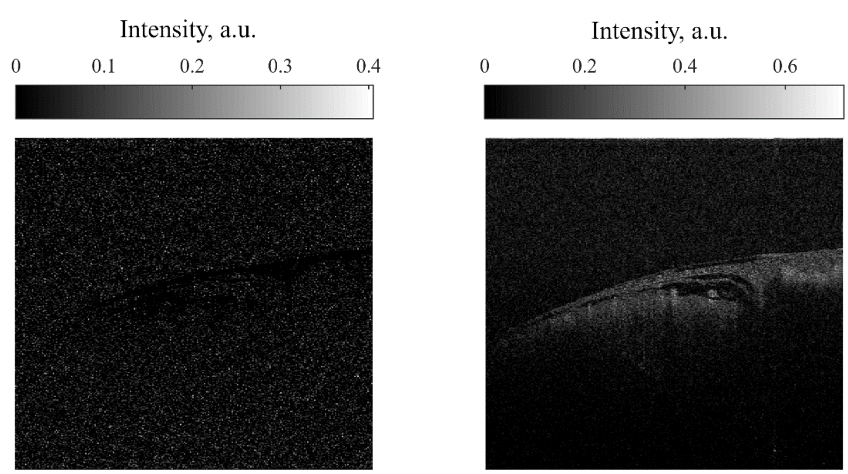

Fig. 12. Speckle variance maps computed before (left) and after (right) intensity adjustment algorithm.

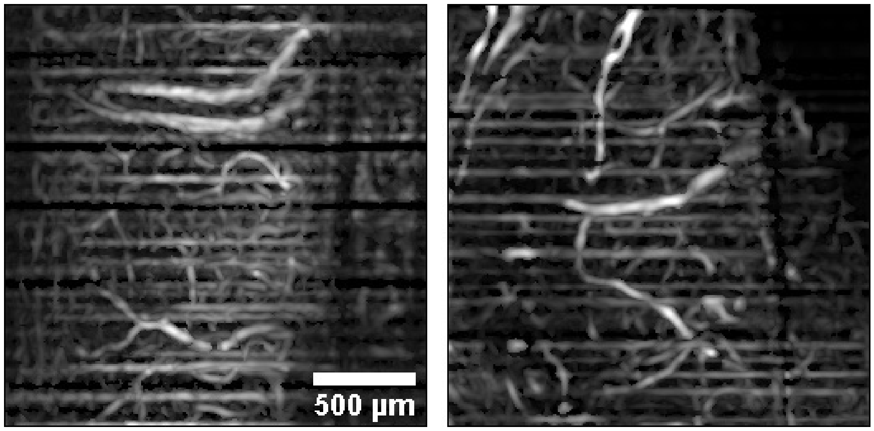

Fig. 13. Maximum intensity projection of superficial cortex layer shows dense vessel topography in both cases of control (left panel) and 8 days developed glioma (right panel).

spots in Fig. 6 on right panel are the blood vessels and they are clearly distinguishable from the semi-static surrounding tissue.

With this algorithm in mind study of vasculature changes in presence of meningeal brain tumor was carried out. Scanning protocol was described as follows: area of the exposed cortex of 2 by 2 mm was probed with the spatial interval of $\sim 8\,\mu$m which is equal to 256 A-lines at a rate of 30 kHz in a single B-scan. Four B-scans were repeatedly acquired in the same spatial location then moving the next region. After scanning each of the B-scan was processed using the proposed intensity correction algorithm, a bundle of four B-scans is then got transformed into one speckle-variance map according to Eq. (1). The final step is to apply a "Tubeness" plugin filter with a sigma value of 3 (Fiji plugin [https://imagej.net/Tubeness]) to enhance the contrast between vessels and surrounding tissues. This filter is designed to compute a Hessian matrix at every pixel of an image and analyze its elements to produce a score for how "tube-like" each point is. Maximum intensity projection of $\sim 400\,\mu$m thick layer of the cortex was done along the axial direction to obtain vessel topography in a case of control (Fig. 13 left panel) and developed glioma (Fig. 13 right panel). Due to relatively low scanning speed of 30 kHz it is required about 30 s to scan along the area of 2 by 2 mm. In such time scales motion artifact are inevitable and as a result, characteristic horizontal stripes of high variance are presented on both images.

6. Perspectives for *in vivo* Studies in Animals and Humans

The developed *in vivo* methods of optical imaging of the cerebral cortex for the analysis of its structural and functional architecture with high spatial-temporal resolution have shown tremendous advantages in studies of neurons, glia and the microvasculature. In animal studies, craniotomy is being widely used to create transparent windows in the skull by completely or partially removing all of these tissues in order to reduce the strong light scattering by the scalp and bone of the skull over the cortex. During long-term experiments, the hole can be periodically closed with a special window.[137]

In medical practice, in some cases, in treating diseases such as brain tumors, subdural or epidural hematomas, hydrocephalus, small holes are drilled in the bones of the human skull, which may be necessary for the insertion of a medical device, removal or biopsy of a brain tumor. Although drilling a hole in the skull is a serious procedure, it is relatively routine.[139] Holes can be repeatedly used. After the holes are no longer needed, they are usually covered with titanium plates.

Such windows can also be used for optical or laser brain irradiation, for example, for the temporary opening of the BBB in the treatment of cancer of the brain, especially in the case of intensive therapy. However, the creation of such windows has significant problems. Therefore, it is desirable to avoid drilling holes in the bones of the skull or thinning it by removing parts of the bone. In 2004, we first proposed to provide optical clearing of the skull bone using immersion optical clearing agents (OCAs).[139] This method, as minimally invasive, found further development in a number of works.[140–142] In the works of Dan Zhu's group, the technology of immersion optical clearing (IOC) of the skull bone received its further development.[143,144] To obtain a clear image of the cerebral cortex, usually four successive stages of the procedure are needed: immobilization of the animal, incision and loosening of the scalp flap, IOC of the cranial bone using an appropriate OCA, and reverse recovery of the optical properties of the skull bone after exposure to saline.

OCA is usually introduced as a thin coupling layer on top of the skull to flatten the surface and induce the optical clearing effect. Thick layers should be avoided because of the fact that Fourier domain OCT systems have limited (by the nature of the detection scheme) imaging depth that do not depends on the optical properties of the sample. Thus, thick OCA will consume the most part of working imaging depth and focusing at the deeper sample's layers will cause an aliasing (overlay of superficial and deep layers of the sample). To perform functional studies with presence of OCA the last should be chosen to provide negligible effect (ideally not affects) on functional parameters such as blood or lymph flow.

In severe cases in humans, in addition to skin incisions, it is possible to drill the entire thickness of the skull bone up to the *dura mater* and bring the distal tip of the fiber directly to the surface of the *dura mater*. Since in medical practice, in some cases, when treating such diseases as brain tumors, small holes are drilled in the bones of the human skull, this hole, made without disrupting the integrity of the *dura mater*, can be used to introduce a fiber for laser irradiation of the deep brain regions to open a BBB and conduct appropriate drug or provide phototherapy, as well as to monitor the results of therapy with endoscopic OCT. The integrity of *dura mater* is very important in terms of maintaining normal intracranial pressure and preventing infection of brain tissue. Drilling a hole in the skull is a fairly routine procedure.[138] Such openings can be multiply reused.

7. Conclusion

The PDT is a promising tool for mini-invasive diagnosis of therapy of brain tumors. The newly discovered effects of PDT on BBB permeability open novel strategies for drug-brain delivery, especially for post-surgical treatment of GBM. This novel knowledge about mechanisms of PDT effects on the permeability of cerebral vessels is an important data for better understanding of PDT-related brain edema, which is the main consequence after PDT of GMB. The newly discovered meningeal lymphatic vessels and their crucial role in brain drainage and clearance system open new strategies for effective prevention of fluid accumulation in the brain after PDT. The augmentation of meningeal lymphatic function might be a promising therapeutic target for preventing of PDT-related brain edema. Non-invasive photonic stimulation of fluid clearance via meningeal lymphatic and application of OCT for bed-side monitoring of meningeal lymphatic drainage have the promising perspectives to be widely applied in both experimental and clinical studies of PDT and improving guidelines of PDT of brain tumors.

Acknowledgments

The experimental results presented in this review was supported by Grants of Russian Science Foundation No. 17-75-20069 (the part included PDT of brain tumor) and No. 18-15-00172 (the part included optical monitoring of lymphatic drainage system of the brain) and Ministry of Science and High Education 17.1223.2017/Pch. VVT was also supported by the Program of Basic Research of the Presidium of the RAS No. 32 "Nanostructures: Physics, Chemistry, Biology, Basic Technologies."

References

1. Q. T. Ostrom, D. J. Cote, M. Ascha, C. Kruchko, J. S. Barnholtz-Sloan, "Adult glioma incidence and survival by race or ethnicity in the United States from 2000 to 2014," *JAMA Oncol.* **4**(9), 1254–1262 (2018).
2. F. Jason, "Pediatric high grade glioma: A review and update on tumor clinical characteristics and biology," *Front Oncol.* **2**, 105 (2012).
3. A. Seker, M. M. Ozek, "Congenital glioblastoma multiforme. Case report and review of the literature," *J. Neurosurg.* **105**, 473–479 (2006).
4. L. C. Hou, S. R. Bababeygy, V. Sarkissian, P. G. Fisher, H. Vogel, P. Barnes, S. L. Huhn, "Congenital glioblastoma multiforme: Case report and review of the literature," *Pediatr. Neurosurg.* **44**, 304–312 (2008).

5. G. M. Milano, C. Cerri, V. Ferruzzi, I. Capolsini, E. Mastrodicasa, L. Genitori, F. Aversa, "Congenital glioblastoma," *Pediatr. Blood Cancer* **53**, 124–126 (2009).
6. A. Broniscer, S. J. Baker, A. N. West, M. M. Fraser, E. Proko, M. Kocak, J. Dalton, G. P. Zambetti, D. W. Ellison, L. E. Kun, A. Gajjar, R. J. Gilbertson, C. E. Fuller, "Clinical and molecular characteristics of malignant transformation of low-grade glioma in children," *J. Clin. Oncol.* **25**, 682–689 (2007).
7. D. N. Louis, H. Ohgaki, O. D. Wiestler, W. K. Cavenee, P. C. Burger, A. Jouvet, B. W. Scheithauer, P. Kleihues, "The 2007 WHO classification of tumours of the central nervous system," *Acta Neuropathol.* **114**, 97–109 (2007).
8. R. Stupp, P. Dietrich, S. Kraljevic, A. Pica, I. Maillard, P. Maeder *et al.*, "Promising survival for patients with newly diagnosed glioblastoma multiforme treated with concomitant radiation plus temozolomide followed by adjuvant temozolomide," *J. Clin. Oncol.* **20**(5), 1375–1382 (2002).
9. P. A. Valdes, F. Leblond, A. Kim, B. T. Harris, B. C. Wilson, X. Fan *et al.*, "Quantitative fluorescence in intracranial tumor: Implications for ALA-induced PpIX as an intraoperative biomarker," *J. Neurosurg.* **115**(1), 11–17 (2011), Epub 2011/03/29.
10. W. Stummer, M. Van den Bent, M. Westphal, "Cytoreductive surgery of glioblastoma as the key to successful adjuvant therapies: New arguments in an old discussion," *Acta Neurochirurgica* **153**(6), 1211–1218 (2011).
11. W. Stummer, H. Stepp, O. D. Wiestler, U. Pichlmeier, "Randomized, prospective double-blinded study comparing 3 different doses of 5-aminolevulinic acid for fluorescence-guided resections of malignant gliomas," *Neurosurgery* **81**(2), 230–239 (2017).
12. R. Crowley, N. Pouratian, J. Sheehan, "Gamma knife surgery for glioblastoma multiforme," *Neurosurg. Focus* **20**(4), E17 (2006).
13. D. Amelio, S. Lorentini, M. Scharwz, M. Amichetti, "Intensity-modulated radiation therapy in newly diagnosed glioblastoma: A systematic review on clinical and technical issues," *Radiother. Oncol.* **97**(3), 361–369 (2010).
14. H. Stepp, T. Beck, T. Pongraz, T. Meinel, F. W. Kreth, J. Ch. Tonn, W. Stummer, "ALA and malignant glioma: Fluorescence-guided resection and photodynamic treatment," *J. Environ. Pathol. Toxicol. Oncol.* **21**, 157–164 (2007).
15. Z. Huang, L. Cheng, O. Guryanova, Q. Wu, S. Bao, "Cancer stem cells in glioblastoma — molecular signaling and therapeutic targeting," *Protein Cell* **1**(7), 638–655 (2010).
16. C. B. Wilson, "Glioblastoma: The past, the present, and the future," *Clin. Neurosurg.* **38**, 32–48 (1992).
17. N. R. Finsen, *Phototherapy*, Edward Arnold, London (1901).
18. O. Raab, "Untersuchungen über die Wirkung fluorescierender Stoffe," *Z. Biol.* **39**, 16 (1899).
19. H. von Tappeiner, A. Jodlbauer, "Über Wirkung der photodynamischen fluorieszierenden Stoffe auf Protozoan und Enzyme," *Dtsch. Arch. Klin. Med.* **80**, 427–487 (1904).
20. F. Meyer-Betz, "Untersuchungen über die biologische photodynamische Wirkung des Hämatoporphyrins und andere Derivate des Blut- und Gallenfarbstoffs," *Dtsch. Arch. Klin. Med.* **112**, 476–450 (1913).
21. T. J. Dougherty, "An update on photodynamic therapy applications," *J. Clin. Laser Med. Surg.* **20**, 3–7 (2002).
22. B. C. Wilson, M. S. Patterson, "The physics, biophysics and technology of photodynamic therapy," *Phys. Med. Biol.* **53**, R61–R109 (2008).
23. A. A. Krasnovsky *et al.*, Singlet oxygen and primary mechanisms of photodynamic therapy and photodynamic diseases, *Photodynamic Therapy at the Cellular Level*, A. B. Uzdensky, Ed., pp. 17–62, Research Signpost, Trivandrum (2007).
24. A. B. Uzdensky *et al.*, "Photodynamic therapy: A review of applications in neurooncology and neuropathology," *J. Biomed. Opt.* **20**(6), 061108 (2015).
25. T. S. Zavadskaya, "Photodynamic therapy in the treatment of glioma," *Exp. Oncol.* **37** 234–241 (2015).
26. G. Shafirstein, D. Bellnier, E. Oakley, S. Hamilton, M. Potasek, K. Beeson, E. Parilov, "Interstitial photodynamic therapy — a focused review," *Cancers* **9**, 12 (2017), doi: 10.3390/cancers 9020012.
27. H. Kostron, T. Hasan, *Photodynamic Medicine from Bench to Clinic, The Royal Society of Chemistry*, Thomas Graham House, Science Park, Milton Road, Cambridge CB4 0WF, UK (2016).
28. A. P. Castano, T. N. Demidova, M. R. Hamblin, "Mechanisms in photodynamic therapy: Part one-photosensitizers, photochemistry and cellular localization," *Photodiagn. Photodyn. Ther.* **1**, 279–293 (2004).
29. M. Hennessy, M. R. Hamblin, "Photobiomodulation and the brain: A new paradigm," *J. Optics* **19**(1), 013–003 (2016).
30. M. S. Eljamel, C. Goodman, H. Moseley, "ALA and Photofrin fluorescence-guided resection and repetitive PDT in glioblastoma multiforme: A

single centre phase III randomised controlled trial," *Lasers Med. Sci.* **23**, 361–367 (2008).
31. P. J. Muller, B. C. Wilson, "Photodynamic therapy of brain tumors — a work in progress," *Lasers Surg. Med.* **38**, 384–389 (2006).
32. Y. Muragaki, J. Akimoto, T. Maruyama, H. Iseki, S. Ikuta, M. Nitta, K. Maebayashi, T. Saito, Y. Okada, S. Kaneko, A. Matsumura, T. Kuroiwa, K. Karasawa, Y. Nakazato, T. Kayama, "Phase II clinical study on intraoperative photodynamic therapy with talaporfin sodium and semiconductor laser in patients with malignant brain tumors," *J. Neurosurg.* **119**, 845–852 (2013).
33. D. Bechet, S. R. Mordon, F. Guillemin, M. A. Barberi-Heyob, "Photodynamic therapy of malignant brain tumors: A complementary approach to conventional therapies," *Cancer Treat. Rev.* **40**, 229–241 (2014).
34. B. J. Quirk, G. Brandal, S. Donlon, J. C. Vera, T. S. Mang, A. B. Foy, S. M. Lew, A. W. Girotti, S. Jogal, P. S. LaViolette, J. M. Connelly, "Whelan HT. Photodynamic therapy (PDT) for malignant brain tumors — where do we stand?," *Photodiagn. Photodyn. Ther.* **12**, 530–544 (2015).
35. L. E. Gasper, B. J. Fisher, D. R. Macdonald, D. V. LeBer, E. C. Halperin, S. C. Schold Jr., J. G. Cairncross, "Supratentorial malignant glioma: Patterns of recurrence and implications for external beam local treatment," *Int. J. Radiai. Oncol. Biol. Phys.* **24**, 55–57 (1992).
36. C. Perria, T. Capuzzo, G. Cavagnaro, R. Datti, N. Francaviglia, C. Rivano, V. E. Tercero, "Fast attempts at the photodynamic treatment of human gliomas," *J. Neurosurg. Sci.* **24**, 119–129 (1980).
37. S. Kaneko, "Safety guidelines for diagnostic and therapeutic laser applications in the neurosurgical feld," *Laser Ther.* **21**, 129–136 (2012).
38. S. S. Stylli, A. H. Kaye, L. MacGregor, M. Howes, P. Rajendra, "Photodynamic therapy of high grade glioma — long term survival," *J. Clin. Neurosci.* **12**, 389–398 (2005).
39. P. J. Muller, B. C. Wilson, "Photodynamic therapy of brain tumor — a work in progress," *Laser Surg. Med.* **38**, 384–389 (2006).
40. H. Kostron, T. Fiegele, E. Akatuna, "Combination of FoSCAN® mediated fluorescence guided resection and photodynamic treatment as a new concept for malignant brain tumors," *Med. Laser Appl.* **21**, 185–290 (2006).
41. S. Eljamel, "Photodynamic applications in brain tumors: A comprehensive review of the literature," *Photodiagn. Photodyn. Ther.* **7**, 76–85 (2010).
42. M. S. Mathews, "Cerebral edema following photodynamic therapy using endogenous and exogenous photosensitizers in normal brain," *Lasers Surg. Med.* **43**, 892–900 (2011).
43. S. S. Stylli, "Photodynamic therapy of cerebral glioma — A review Part I — A biological basis," *J. Clin. Neurosci.* **13**, 615–625 (2006).
44. H. Hirschberg, "Disruption of the blood–brain barrier following ALA-mediated photodynamic therapy," *Lasers Surg. Med.* **40**, 535–542 (2008).
45. S. J. Madsen, "Site-specific opening of the blood-brain barrier," *J. Biophoton.* **3**, 356–367 (2010).
46. S. J. Madsen, "Increased nanoparticle-loaded exogenous macrophage migration into the brain following PDT-induced blood-brain barrier disruption," *Lasers Surg. Med.* **45**, 524–532 (2013).
47. S. J. Madsen, "Nanoparticle-loaded macrophage-mediated photothermal therapy: Potential for glioma treatment," *Lasers Med. Sci.* **4**, 1357–1365 (2015).
48. C. Zhang, W. Feng, Y. Li, J. Kürths, T. Yu, O. Semyachkina-Glushkovskaya, D. Zhu, "Age differences in photodynamic opening of blood-brain barrier through optical clearing skull window in mice," *Lasers Surg. Med.* (2019), doi: 10.1002/lsm.23075.
49. Ch. Zhang, W. Feng, E. Vodovosova, D. Tretiakova, I. Boldyrev, Yu. Li, Ju. Kurths, T. Yu, O. Semyachkina-Glushkovskaya, D. Zhu, "Photodynamic opening of the blood-brain barrier to high weight molecules and liposomes through an optical clearing skull window," *Biomed. Opt. Express* **9**, 4850–4862 (2018).
50. O. Semyachkina-Glushkovskaya, J. Kurths, E. Borisova, S. Sokolovsky, N. Mantareva, I. Angelov, A. Shirokov, N. Navolokin, N. Shushunova, A. Khorovodov, M. Ulanova, M. Sagatova, I. Ahranovich, O. Sindeeva, A. Gekalyuk, A. Bordova, E. Rafailov, "Photodynamic opening of blood-brain barrier," *Biomed. Opt. Express* **8**(11) (2017) https://doi.org/10.1364/BOE.8.005040.
51. N. J. Abbott, "Astrocyte-endothelial interactions at the blood–brain barrier," *Nat. Rev. Neurosci.* **7**, 41–53 (2006).
52. P. Balabh, "The blood-brain barrier: An overview structure, regulation, and clinical implication," *Neurobiol. Dis.* **16**, 1–13 (2004).
53. H. Wolburg, "Tight junctions of the blood–brain barrier: Development, composition and regulation," *Vascul. Pharmacol.* **38**, 323–337 (2002).
54. K. Matter, "Signalling to and from tight junctions," *Nat. Rev. Mol. Cell Biol.* **4**, 225–236 (2003).
55. H. Wolburg, "Brain endothelial cells and the glio–vascular complex," *Cell Tissue Res.* **335**, 75–96 (2009).
56. B. T. Hawkins, "The blood–brain barrier/neurovascular unit in health and disease," *Pharmacol. Rev.* **57**, 173–185 (2005).

57. N. J. Abbott, A. A. K. Patabendige, D. E. M. Dolman, S. R. Yusof, D. J. Begley, "Structure and function of the blood-brain barrier," *Neurobiol. Dis.* **37**, 13–25 (2010).
58. W. M. Pardridge, "Molecular Trojan horses for blood-brain barrier drug delivery," *Curr. Opin. Pharmacol.* **6**, 494–500 (2006).
59. D. Silberberg, N. P. Anand, K. Michels, R. N. Kalaria, "Brain and other nervous system disorders across the lifespan — global challenges and opportunities," *Nature* **527**, 151–154 (2015).
60. M. M. Patel, B. M. Patel, "Crossing the Blood-Brain Barrier: Recent Advances in Drug Delivery to the Brain," *CNS Drugs* **31**, 109–133 (2017).
61. S. Mitragotri, "Devices for overcoming biological barriers: The use of physical forces to disrupt the barriers," *Adv. Drug Deliv. Rev.* **65**, 100–103 (2013).
62. D. S. Hersh, A. S. Wadajkar, N. B. Roberts, J. G. Perez, N. P. Connolly, V. Frenkel, J. A. Winkles, G. F. Woodworth, A. J. Kim, "Evolving drug delivery strategies to overcome the blood brain barrier," *Curr. Pharm. Design* **22**, 1177–1193 (2016).
63. F. Celine, "Innovations of photodynamic therapy for brain tumors: Potential of multifunctional nanoparticles" *J. CarcinogeneMutagene* **8**, 1–7 (2012).
64. A. J. Trinidad, "Combined concurrent photodynamic and gold nanoshell loaded macrophage-mediated photothermal therapies: An in vitro study on squamous cell head and neck carcinoma," *Lasers Surg Med.* **4**, 310–318 (2014).
65. V. H. Fingar, "Vascular effects of photodynamic therapy," *J. Clin. Laser Med. Sur.* **14**(5), 323–328 (1996).
66. S. S. Hu, H. B. Cheng, Y. R. Zheng, R. Y. Zhang, W. Yue, H. Zhang, "Effects of photodynamic therapy on the ultrastructure of glioma cells," *Biomed. Environ. Sci.* **20**(4), 269–273 (2007).
67. L. A. Sporn, T. H. Foster, "Photofrin and light induces microtubule depolymerization in cultured human endothelial cells," *Cancer Res.* **52**(12), 3443–3448 (1992).
68. P. Agostinis, K. Berg, K. A. Cengel *et al.*, "Photodynamic therapy of cancer: An update," *Ca-a Cancer J. Clin.* **61**(4), 250–281 (2011).
69. Y. Kusama, M. Bernier, D. J. Hearse, "Singlet oxygen-induced arrhythmias. Dose- and light-response studies for photoactivation of rose bengal in the rat heart," *Circulation* **80**(5), 1432–1448 (1989).
70. G. Vandeplassche, M. Bernier, F. Thone, M. Borgers, Y. Kusama, D. J. Hearse, "Singlet oxygen and myocardial injury: Ultrastructural, cytochemical and electrocardiographic consequences of photoactivation of rose Bengal," *J. Mol. Cell Cardiol.* **22**(3), 287–301 (1990).
71. F. Yoshino, H. Shoji, M. C. I. Lee, "Vascular effects of singlet oxygen (O-1(2)) generated by photo-excitation on adrenergic neurotransmission in isolated rabbit mesenteric vein," *Redox. Rep.* **7**(5):266–270 (2002).
72. M. R. Hara, J. J. Kovacs, E. J. Whalen, S. Rajagopal, R. T. Strachan, W. Grant, A. J. Towers, B. Williams, C. M. Lam, K. Xiao, S. K. Shenoy, S. G. Gregory, S. Ahn, D. R. Duckett, R. J. Lefkowitz, "A stress response pathway regulates DNA damage through beta(2)-adrenoreceptors and beta-arrestin-1," *Nature*, **477**, 349–353 (2011).
73. R. J. Leftowitz, S. K. Shenoy, "Transduction of receptor signals by beta-arrestins," *Science*, **308**, 512–517 (2005).
74. J. K. Hebda, H. M. Leclair, S. Azzi, C. Roussel, M. G. Scott, N. Bidère, J. Gavard, "The C-terminus region of β-arrestin1 modulates VE-cadherin expression and endothelial cell permeability," *Cell Commun. Signal.* **11**, 1–7 (2013).
75. S. S. Hu, H. B. Cheng, Y. R. Zheng, R. Y. Zhang, W. Yue, H. Zhang, "Effects of photodynamic therapy on the ultrastructure of glioma cells," *Biomed. Environ. Sci.* **20**, 269–273 (2007).
76. H. Ito, H. Matsui, "Mitochondrial reactive oxygen species and photodynamic therapy," *Laser Ther.* **25**, 193–199 (2016).
77. H. Buzza, L. C. F. de Fraitas, L. T. Moriayama, R. Rosa, F. Bagnato, C. Kurachi, "Vascular effects of photodynamic therapy with circumin in a chlorioallantoic membrane model," *Int. J. Mol. Sci.* **20**(5), 1084 (2019).
78. J. W. Snyder, W. R. Greco, D. A. Bellnier, L. Vaughan, B. W. Henderson, "Photodynamic therapy: A means to enhanced drug delivery to tumors," *Cancer Res.* **63**, 8126–8131 (2003).
79. E. Debefve, B. Pegaz, J. P. Ballini, Y. N. Konan, H. Van den Bergh, "Combination therapy using aspirin enhanced photodynamic selective drug delivery," *Vasc. Pharmacol.* **46**, 171–180 (2007).
80. E. Debefve, B. Pegaz, H. van den Bergh, G. Wagnieres, N. Lange, J. P. Ballini, "Video monitoring of neovessel occlusion induced by photodynamic therapy with verteporfin (Visudyne), in the CAM model," *Angiogenesis.* **2008**, 235–243 (2008).
81. W. Stummer, C. Goetz, A. Hassan, D. V. M Heimann, O. Kempski, "Kinetics of Photofrin II in perifocal brain edema," *Neurosurgery.* **33**, 1075–1082 (1993).
82. C. Goetz, A. Hasan, W. Stummer, A. Heimann, O. Kempski, "Experimental research photodynamic effects in perifocal, oedematous brain

tissue," *Acta Neurochir (Wien)* **144**(2), 173–179 (2002).

83. S. Ito, W. Rachinger, H. Stepp, H. J. Reulen, W. Stummer, "Oedema formation in experimental photoirradiation therapy of brain tumours using 5-ALA," *Acta Neurochir (Wien)* **147**(1), 57–65 (2005).
84. M. Westphal, "5-aminolevulinic acid induced endogenous porphyrin fluorescence in 9L and C6 brain tumours and in the normal rat brain — Comment," *Acta Neurochir* **140**(5), 512–513 (1998).
85. A. S. Filippidis, R. B. Carozza, H. L. Rekate, "Aquaporins in brain edema and neuropathological conditions," *Int. J. Mol. Sci.* **18**(1), 55 (2017).
86. S. Michinaga, Y. Koyama, "Pathogenesis of brain edema and investigation into anti-edema drugs," *Int. J. Mol. Sci.* **16**(5), 9949–9975 (2015).
87. H. F. Cserr, C. S. Patlak, "Secretion and bulk flow of interstitial fluid," in *Physiology and Pharmacology of the Blood-Brain Barrier*, ed. M. W. B. Bradbury (Berlin: Springer-Verlag, 1992), pp. 245–261.
88. H. Davson, M. B. Segal, *Physiology of the CSF and Blood-brain Barriers* (Boca Raton: CRC Press, 1996).
89. M. W. Bradbury, "Lymphatics and the central nervous system," in *Trends Neuroscience* (Cambridge: Cell Press, 1981), pp. 100–101.
90. M. W. B. Bradbury, R. J. Westrop, "Factors influencing exit of substances from cerebrospinal-fluid into deep cervical lymph of the rabbit," *J. Physiol.* **339**, 519–534 (1983).
91. S. Kida, A. Pantazis, R. O. Weller, "CSF drains directly from the subarachnoid space into nasal lymphatics in the rat — anatomy, histology and immunological significance," *Neuropathol. Appl. Neurobiol.* **19**, 480–488 (1993).
92. M. Johnston, C. Papaiconomou, "Cerebrospinal fluid transport: A lymphatic perspective," *News Physiol. Sci.* **17**, 227–230 (2002).
93. M. Johnston, A. Zakharov, C. Papaiconomou, G. Salmasi, D. Armstrong, "Evidence of connections between cerebrospinal fluid and nasal lymphatic vessels in humans, non-human primates and other mammalian species," *Cerebrospinal Fluid Res.* **1**:2 (2004). doi: 10.1186/1743-8454-1-2.
94. N. J. Abbott, "Evidence for bulk flow of brain interstitial fluid: Significance for physiology and pathology," *Neurochem. Int.* **45**, 545–552 (2004).
95. R. O. Weller, E. Djuanda, H.-Y. Yow, R. O. Carare, "Lymphatic drainage of the brain and the pathophysiology of neurological disease," *ActaNeuropathol.* **117**, 1–14 (2009).
96. L. Koh, A. Zakharov, M. Johnston, "Integration of the subarachnoid space and lymphatics: Is it time to embrace a new concept of cerebrospinal fluid absorption?" *Cerebrospinal Fluid Res.* **2**:6 (2005). doi: 10.1186/1743-8454-2-6.
97. H. F. Cserr, P. M. Knopf, "Cervical lymphatics, the blood-brain barrier and the immureactivity of the brain: A new view," *Immunol. Today.* **13**(12), 507–512 (1992).
98. M. Lohrberg, J. Wilting, "The lymphatic vascular system of the mouse head," *Cell Tissue Res.* **366**, 667–677 (2016), doi: 10.1007/s00441-016-2493-8.
99. W. His, "UebereinperivaskulaeresKanalsystem in den nervoesen Central-Organen und ueberdessen Beziehungenzum Lymphsystem," *Z. WissZool.* **5**, 127–141 (1865).
100. G. Schwalbe, "Die Arachnoidalraum, einLymphraum und sein Zusammenhangmit den Perichorioidalraum," *Zentralbl. Med. Wiss.* **7**, 465–467 (1869).
101. L. H. Weed, "The pathways of escape from the subarachnoid spaces with particular reference to the arachnoid villi," *J. Med. Res.* **31**, 51–91 (1914).
102. J. F. Iliff, M. Wang, Y. Liao, B. A. Plogg, W. Peng, G. A. Gundersen, H. Benveniste, G. E. Vates, R. Deane, S. A. Goldman, E. A. Nagelhus, M. Nedergaard, "A paravascular pathway facilitates CSF flow through the brain parenchyma and the clearance of interstitial solutes, including amyloid β," *Sci. Transl. Med.* **366**, 667–677 (2012). doi: 10.1126/scitranslmed.3003748.
103. R. T. Jackson, J. Tigges, W. Arnold, "Subarachnoid space of the CNS, nasal mucosa, and lymphatic system," *Arch. Otolaryngol.* **105**, 180 (1979).
104. A. Aspelund, S. Antila, S. T. Proulx, T. V. Karlsen, S. Karaman, M. Detmar, H. Wiig, K. Alitalo, "A dural lymphatic vascular system that drains brain interstitial fluid and macromolecules," *J. Exp. Med.* **212**, 991–999 (2015), doi: 10.1084/jem.20142290.
105. A. Louveau, I. Smirnov, T. J. Keyes, J. D. Eccles, S. J. Rouhani, J. D. Peske, N. C. Derecki, D. Castle, J. W. Mandell, K. S. Lee, T. H. Harris, J. Kipnis, "Structural and functional features of central nervous system lymphatic vessels," *Nature* **523**, 337–341 (2015), doi: 10.1038/nature14432.
106. O. Semyachkina-Glushkovskaya, A. Abdurashitov, A. Dubrovsky, D. Bragin, O. Bragina, N. Shushunova, G. Maslyakova, N. Navolokin, A. Bucharskaya, V. Tuchin, J. Kurths, "Application of optical coherent tomography for *in vivo* monitoring of the meningeal lymphatic vessels during opening of blood-brain barrier: Mechanisms of brain clearing,"

J. Biomed. Opt. (2017), doi: 10.1117/1.JBO.22. 12.121719.

107. O. Semyachkina-Glushkovskaya, V. Chehonin, E. Borisova, I. Fedosov, A. Namykin, A. Abdurashitov, A. Shirokov, B. Khlebtsov, Y. Lyubun, N. Navolokin, M. Ulanova, N. Shushunova, A. Khorovodov, I. Agranovich, A. Bodrova, M. Sagatova, A. Esmat, E. Shareef Saranceva, T. Iskra, M. Dvoryatkina, E. Zhinchenko, O. Sindeeva, V. Tuchin, J. Kurths, "Photodynamic opening of the blood-brain barrier and pathways of brain clearing pathways," *J. Biophoton.* (2018), doi: 10.1002/jbio.201700287.
108. B. Mokri, "The Monro-Kellie hypothesis: Applications in CSF volume depletion," *Neurology.* **56**(12), 1746–1748 (2001).
109. L. Liu, K. Duff, "A technique for serial collection of cerebrospinal fluid from the cisterna magna in mouse," *JoVE.* **21** (2008), doi: 10.3791/960.
110. O. Semyachkina-Glushkovskaya, J. Kurths, E. Borisova, S. Sokolovsky, N. Mantareva, I. Angelov, A. Shirokov, N. Navolokin, N. Shushunova, A. Khorovodov, M. Ulanova, M. Sagatova, I. Ahranovich, O. Sindeeva, A. Gekalyuk, A. Bordova, E. Rafailov, "Photodynamic opening of blood-brain barrier," *Biomed. Opt. Express.* **8**, 11 (2017), doi: 10.1364/BOE. 8.005040.
111. P. Batuk, J. Fuxe, H. Hashizume, T. Romano, E. Lashnits, S. Butz, D. Vestweber, M. Corada, C. Molendinin, E. Dejana, "Functionally specialized junctions between endothelial cells of lymphatic vessels," *J. Exp. Med.* **204**, 2349–2362 (2004).
112. C. Kesler, S. Kiao, L. Munn, T. Padera, "Lymphatic vessels in health and diseases," *Wiley Interdiscip. Rev. Syst. Biol. Med.* **5**(1), 111–124 (2013). doi: 10.1002/wsbm.1201.
113. C. Greene, M. Campbell, "Tight junction modulation of the blood brain barrier: CNS delivery of small molecules," *Tissue Barriers.* **4**(1), e1138017 (2016). doi: 10.1080/21688370.2015. 1138017.
114. J. Scallan, S. Zawieja, J. Castorena-Gonzalez, M. Davis, "Lymphatic pumping: Mechanics, mechanisms and malfunction," *J. Physiol.* **594**, 5749–5768 (2016). doi: 10.1113/JP272088.
115. T. Ohhashi, R. Mizuno, F. Ikomi, Y. Kawai, "Current topics of physiology and pharmacology in the lymphatic system," *Pharmacol. Ther.* **105**, 165–188 (2005).
116. H. G. Bohlen, O. Y. Gasheva, D. C. Zawieja, "Nitric oxide formation by lymphatic bulb and valves is a major regulatory component of lymphatic pumping," *Am. J. Physiol. Heart Circ. Physiol.* **301**, H1897–1906 (2011). doi: 10.1152/ ajpheart.00260.2011.
117. J. Eisenhoffer, Z. Y. Yuan, M. G. Johnston, "Evidence that the L-arginine pathway plays a role in the regulation of pumping activity in bovine mesenteric lymphatic vessels," *Microvasc. Res.* **50**, 249–259 (1995).
118. O. Y. Gasheva, D. C. Zawieja, A. A. Gashev, "Contraction-initiated NO-dependent lymphatic relaxation: A self-regulatory mechanism in rat thoracic duct," *J. Physiol.* **575**, 821–832 (2006).
119. Y. Shirasawa, F. Ikomi, T. Ohhashi, "Physiological roles of endogenous nitric oxide in lymphatic pump activity of rat mesentery *in vivo*," *Am. J. Physiol. Gastrointest. Liver Physiol.* **278**, G551–556 (2000).
120. A. Koller, R. Mizuno, G. Kaley, "Flow reduces the amplitude and increases the frequency of lymphatic vasomotion: Role of endothelial prostanoids," *Am. J. Physiol.* **277**, R1683-1689 (1999).
121. S. Da Mesquita, A. Louveau, A. Vaccari, I. Smirnov, R. C. Cornelison, K. M. Kingsmore, C. Contarino, S. Onengut-Gumuscu, E. Farber, D. Raper, K. E. Viar, R. D. Powell, W. Baker, N. Dabhi, R. Bai, R. Cao, S. Hu, S. S. Rich, J. M. Munson, M. B. Lopes, C. C. Overall, S. T. Acton and J. Kipnis, "Functional aspects of meningeal lymphatics in ageing and Alzheimer's disease," *Nature* **560**, 185–191 2018.
122. M. Absinta1, S.-K. Ha, G. Nair, P. Sati, N. J. Luciano, M. Palisoc, A. Louveau, K. A. Zaghloul, S. Pittaluga, J. Kipnis, D. S. Reich, "Human and nonhuman primate meninges harbor lymphatic vessels that can be visualized noninvasively by MRI," *eLife* **6**, e29738 (2017), doi: https://doi.org/ 10.7554/eLife.29738.
123. V. V. Tuchin, *Tissue Optics: Light Scattering Methods and Instruments for Medical Diagnosis*, 3rd ed., PM 254 (SPIE Press, Bellingham, WA, 2015), 988 p.
124. W. Drexler, J. G. Fujimoto (eds.), *Optical Coherence Tomography: Technology and Applications*, 2nd ed. (Springer International Publishing, Switzerland, 2015), 2571 p.
125. C. J. Liu, G. A. Shamsan, T. Akkin, D. J. Odde, "Glioma cell migration dynamics in brain tissue assessed by multimodal optical imaging," *Biophys. J.* **117**(7), 1179–1188 (2019).
126. Y. Fan, Y. Xia, X. Zhang, Y. Sun, J. Tang, L. Zhang, H. Liao, "Optical coherence tomography for precision brain imaging, neurosurgical guidance and minimally invasive theranostics," *Biosci. Trends* **12**(1), 12–23 (2018).
127. R. M. Nolan, S. G. Adie, M. Marjanovic, E. J. Chaney, F. A. South, G. L. Monroy, D. G. Simpson, "Intraoperative optical coherence tomography for assessing human lymph nodes for metastatic cancer," *BMC Cancer* **16**(1), 144 (2016).

128. H. Ramakonar, B. C. Quirk, R. W. Kirk, J. Li, A. Jacques, C. R. Lind, R. A. McLaughlin, "Intraoperative detection of blood vessels with an imaging needle during neurosurgery in humans," *Sci. Adv.* **4**(12), eaav4992 (2018).
129. W. Drexler, J. G. Fujimoto (ed.), *Optical Coherence Tomography: Technology and Applications* (Springer Science & Business Media, 2008).
130. M. Hagen-Eggert, P. Koch, G. Hüttmann, "Analysis of the signal fall-off in spectral domain optical coherence tomography systems," in *Optical Coherence Tomography and Coherence Domain Optical Methods in Biomedicine XVI*, Vol. 8213 (International Society for Optics and Photonics, 2012, February), p. 82131K.
131. A. Federici, A. Dubois, "Full-field optical coherence microscopy with optimized ultrahigh spatial resolution," *Opt. Lett.* **40**(22), 5347–5350 (2015).
132. L. Tong, Q. Wei, A. Wei, J. X. Cheng, "Gold nanorods as contrast agents for biological imaging: Optical properties, surface conjugation and photothermal effects," *Photochem. Photobiol.* **85**(1), 21–32 (2009).
133. O. Liba, E. D. SoRelle, D. Sen, A. de La Zerda, "Contrast-enhanced optical coherence tomography with picomolar sensitivity for functional *in vivo* imaging," *Sci. Rep.* **6**, 23337 (2016).
134. E. D. SoRelle, O. Liba, Z. Hussain, M. Gambhir, A. de la Zerda, "Biofunctionalization of large gold nanorods realizes ultrahigh-sensitivity optical imaging agents," *Langmuir* **31**(45), 12339–12347 (2015).
135. A. L. Oldenburg, M. N. Hansen, A. Wei, S. A. Boppart, "Plasmon-resonant gold nanorods provide spectroscopic OCT contrast in excised human breast tumors," in *Molecular Probes for Biomedical Applications II*, Vol. 6867 (International Society for Optics and Photonics, 2008, February), p. 68670E.
136. C. L. Chen, R. K. Wang, "Optical coherence tomography based angiography," *Biomed. Opt. Express* **8**(2), 1056–1082 (2017).
137. A. Y. Shih *et al.*, "Polished and Reinforced Thinned-skull Window for the Mouse Brain," *J. Visual. Exp.* **61**, e3742, 1–6 (2012).
138. https://www.healthline.com/health/burr-hole (accessed 08/12/2019).
139. A. N. Bashkatov *et al.*, "Optical clearing of human cranial bones," in *Biophotonics: From Fundamental Principles to Health, Environment, Security & Defense Applications* (Ottawa, Ontario, Canada, September 29–October 9, 2004).
140. V. V. Tuchin, *Optical Clearing of Tissues and Blood, PM 154* (SPIE Press, Bellingham, WA, 2006).
141. E. A. Genina, A. N. Bashkatov, V. V. Tuchin, "Optical Clearing of Cranial Bone," *Adv. Opt. Technol.* Article ID 267867, 8 (2008).
142. D. Zhu, K. V. Larin, Q. Luo, V. V. Tuchin, "Recent progress in tissue optical clearing," *Laser Photon. Rev.* **7**(5), 732–757 (2013), doi: 10.1002/lpor.201200056.
143. J. Wang, Y. Zhang, T. Xu, Q. Luo, D. Zhu, "An innovative transparent cranial window based on skull optical clearing," *Laser Phys. Lett.* **9**, 469–473 (2012).
144. Y.-J. Zhao *et al.*, "Skull optical clearing window for in vivo imaging of the mouse cortex at synaptic resolution," *Light: Sci. Appl.* **7**, e17153 (2018), doi: 10.1038/lsa.2017.153.